

Alloying Gold with Copper Makes for a Highly Selective Visible-Light Photocatalyst for the Reduction of Nitroaromatics to Anilines

Qi Xiao,[†] Sarina Sarina,[†] Eric R. Waclawik,[†] Jianfeng Jia,[‡] Jin Chang,^{†,§} James D. Riches,^{||} Haishun Wu,[‡] Zhanfeng Zheng,[⊥] and Huaiyong Zhu^{*,†}

[†]School of Chemistry, Physics and Mechanical Engineering, Science and Engineering Faculty, Queensland University of Technology, Brisbane, QLD 4001, Australia

[‡]School of Chemical and Material Science, Shanxi Normal University, Linfen 041004, China

[§]Institute of Advanced Materials (IAM), National Jiangsu Synergistic Innovation Center for Advanced Materials (SICAM), Nanjing Tech University, Nanjing 211816, China

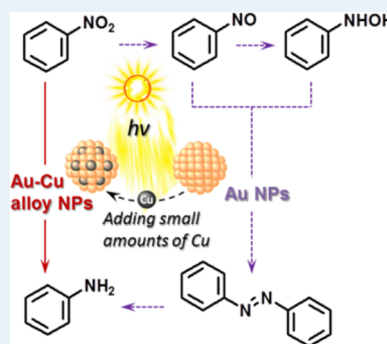
^{||}Institute for Future Environments & School of Earth, Environmental and Biological Sciences, Queensland University of Technology, Brisbane, QLD 4001, Australia

[⊥]State Key Laboratory of Coal Conversion, Institute of Coal Chemistry, Taiyuan 030001, China

S Supporting Information

ABSTRACT: Finely control of product selectivity is an essential issue in organic chemical production. In the synthesis of functionalized anilines via reduction of the corresponding nitroarenes, the challenge is to selectively reduce only the nitro group in the presence of other reducible functional groups in nitroarene molecules at a high reaction rate. Normally, the nitroarene is reduced stepwise through a series of intermediates that remain as byproducts, increasing the aniline synthesis cost. Here we report that alloying small amounts of copper into gold nanoparticles can alter the reaction pathway of the catalytic reduction under visible-light irradiation at ambient temperature, allowing nitroaromatics to be transformed directly to anilines in a highly selective manner. The reasons for the high efficiency of the photocatalytic reduction under these comparatively benign conditions as well as the light-excited reaction mechanisms are discussed. This photocatalytic process avoids byproducts, exhibits a high reaction rate and excellent substituent tolerance, and can be used for the synthesis of many useful functionalized anilines under environmentally benign conditions. Switching of the reaction pathway simply by tailoring the bimetallic alloy NPs of the photocatalysts is effective for engineering of product chemoselectivity.

KEYWORDS: Au–Cu alloy, photocatalysis, reduction, reaction pathways, visible light



INTRODUCTION

Nitroaromatic compounds are among the most important industrial chemicals in use today.¹ For example, approximately 95% of nitroarenes are consumed in the production of anilines, which are important precursors to rubber chemicals, pesticides, dyes, explosives, and pharmaceuticals.² An essential issue with this reduction process is achieving high product selectivity.^{3–6} Many useful anilines contain reducible functional groups. It is a challenge to reduce only the nitro group at a high reaction rate while maintaining any other reducible groups in the reactants unchanged.^{3,5,6} The selective reduction process has been extensively studied using a variety of heterogeneous catalytic systems.^{3–6} In those reported catalytic systems, the reduction proceeds via the well-known pathways first proposed by Haber in 1898 (Figure 1).⁷ The nitro group of the reactant is reduced to the corresponding aniline in a stepwise manner through nitroso and hydroxylamine intermediates.^{8–11} Condensation of the reactive intermediates yields coupling derivatives such as azobenzene and azoxybenzene,^{10,11} but the conversions from the azoxy compound to the azo compound and from the azo

compound to the aniline are slow steps.¹¹ These steps involve cleavage of the last O–N bond and addition of H to the azo group, respectively, and high reaction temperatures and high pressures of hydrogen are used to accelerate these processes, even though excellent catalysts have been discovered. These conditions can reduce other functional groups in the reactants.

We previously reported that Au nanoparticles (NPs) supported on catalytically inert zirconium oxide (ZrO₂) can exhibit high catalytic activity for the selective transformation of nitroaromatics to the corresponding azo compounds in isopropanol solution under visible-light irradiation at 40 °C.¹² The supported Au NPs strongly absorb visible light by means of the localized surface plasmon resonance (LSPR) effect and efficiently channel the light energy to the reactant, inducing reaction under moderate reaction conditions.^{13–15} The photocatalytic reduction using supported Au NPs also proceeds via

Received: November 22, 2015

Revised: January 18, 2016

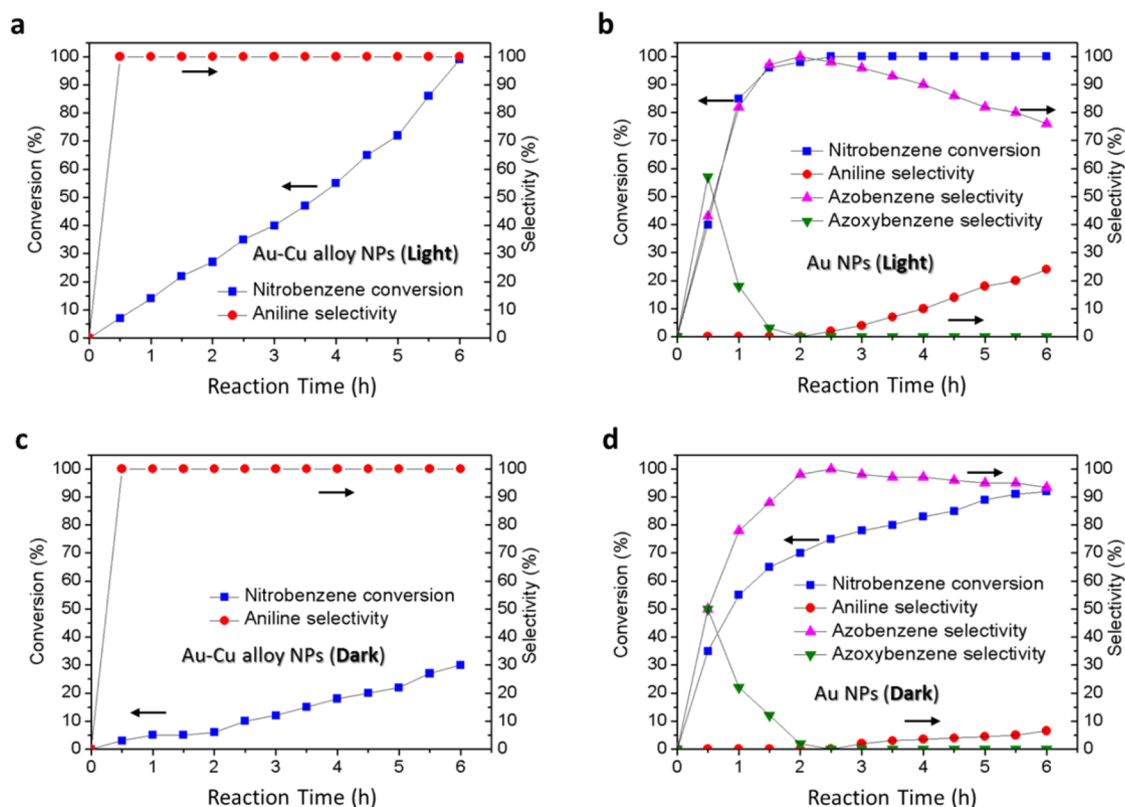


Figure 3. (a, b) Time-conversion plots for nitrobenzene reduction under visible-light irradiation using (a) $\text{Au}_{2.6}\text{Cu}_{0.4}/\text{ZrO}_2$ and (b) $\text{Au}_{3.0}/\text{ZrO}_2$ as the catalyst. (c, d) Time-conversion plots for nitrobenzene reduction in the dark using (c) $\text{Au}_{2.6}\text{Cu}_{0.4}/\text{ZrO}_2$ and (d) $\text{Au}_{3.0}/\text{ZrO}_2$ as the catalyst. The reactions were conducted in an argon atmosphere at 40 °C using 2 mL of isopropyl alcohol mixed with 0.025 mmol of KOH, 0.1 mmol of nitrobenzene, and 50 mg of catalyst. The irradiation intensity was 0.5 W/cm², and the reaction time was 6 h. For the dark reactions, all the reaction conditions were identical to those for the photocatalytic reactions except that the reaction tubes were kept out of the light.

process with the pure Au NP catalyst indicates that the photocatalytic coupling follows the pathways proposed by Haber.^{7,10,11} In contrast, the reduction catalyzed by Au-Cu alloy NPs does not.

The photocatalytic coupling of nitrobenzene on the pure Au NP surface does not consume the reducing agent except in the initial stage,¹² while the direct reduction of nitrobenzene to aniline should. Isopropyl alcohol was the reducing agent in the photocatalytic reduction, which provided hydrogen and was oxidized to acetone. The content of acetone in the reaction system catalyzed by the Au-Cu alloy NPs increased gradually as the reaction proceeded (Figure 4), in proportion with the

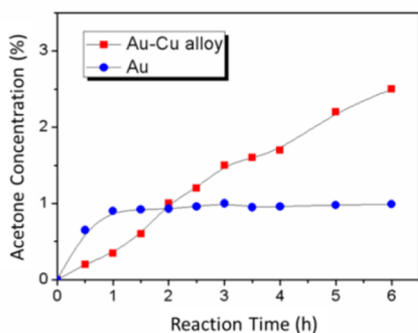


Figure 4. Time-conversion plots for acetone formation during the reduction of nitrobenzene under visible-light irradiation using the $\text{Au}_{2.6}\text{Cu}_{0.4}/\text{ZrO}_2$ and $\text{Au}_{3.0}/\text{ZrO}_2$ catalysts.

aniline yield. Both reactants exist in the liquid phase and have adequate access to the catalyst dispersed in the liquid. This is part of the reason why the reaction can proceed at ambient pressure, which leads to significant savings in the cost of the reactor. The catalyst can be readily recycled after reactions without significant loss of activity (for details, see Figure S1 in the Supporting Information (SI)).

Figure 5a shows a typical transmission electron microscopy (TEM) image of the $\text{Au}_{2.6}\text{Cu}_{0.4}/\text{ZrO}_2$ catalyst. The mean size of the alloy NPs was 5 nm. The lattice fringes of the Au-Cu alloy NPs can be observed in the high-resolution TEM (HR-TEM) image in Figure 5b. The lattice fringe spacing of 0.22 nm corresponds to the interplanar distance of Au-Cu alloy (111) planes.¹⁶ Energy-dispersive X-ray spectroscopy (EDS) line scan analysis of a Au-Cu alloy NP indicated that Au and Cu were uniformly distributed in the alloy NP (Figure 5a inset). This was also apparent in the EDS mapping and X-ray photoelectron spectroscopy (XPS) analysis provided in Figures S2 and S3 in the SI, which showed that the Au content was much higher than the Cu content. The characterization results confirmed the formation of $\text{Au}_{2.6}\text{Cu}_{0.4}$ alloy NPs.

A challenge for Cu-based NP catalysts is that O_2 in air can oxidize surface Cu atoms of the alloy NPs, which results in a rapid loss of activity during reactions exposed to air.¹⁷ It is known that the Cu oxidation rate depends on the alloy NP composition and that increasing amounts of Au can improve the stability of the catalyst.¹⁸ In bulk Au-Cu alloys, Au can protect Cu from oxidation by limiting Cu_2O surface island growth.¹⁹ Thus, we anticipated that Au-Cu alloy NPs with a

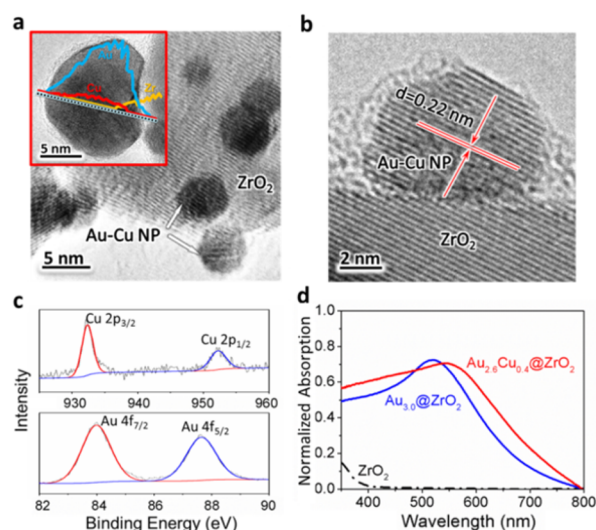


Figure 5. Characterization of the photocatalyst. (a) Typical TEM image of $\text{Au}_{2.6}\text{Cu}_{0.4}@\text{ZrO}_2$. The inset shows a line profile analysis providing information about the elemental composition and Au/Cu distribution of the NP. (b) HR-TEM image of a typical $\text{Au}_{2.6}\text{Cu}_{0.4}$ alloy NP. (c) XPS profiles of Cu and Au species in the $\text{Au}_{2.6}\text{Cu}_{0.4}$ alloy NPs. (d) UV/vis spectra of the $\text{Au}_{2.6}\text{Cu}_{0.4}@\text{ZrO}_2$ and monometallic $\text{Au}_{3.0}@\text{ZrO}_2$ catalysts.

low Cu content would be stable in air. The XPS spectra in Figure 5c confirmed this. The binding energies of Cu $2p_{1/2}$ at around 952.0 eV and Cu $2p_{3/2}$ at 932.5 eV can be mainly attributed to the Cu^0 state.^{20,21} However, because of the low loading of Cu and low signal intensity, analysis of the Cu Auger lines to assign Cu^0 and Cu^+ was not possible.²² Sugano et al.²³ suggested that in the Au–Cu alloy NP photocatalyst the partially oxidized surface Cu atoms could be successfully reduced by plasmon-activated Au atoms to maintain the Au–Cu alloying effect. Thus, even if a very small amount of copper oxide exists on the surface, it could be reduced to the metallic state under irradiation.^{23,24} The binding energies for Au are identical to those in bulk gold metal.²⁵

The light absorption property is an important characteristic of a photocatalyst. The monometallic Au NP catalyst exhibits a distinctive light absorption band at 525 nm due to the LSPR effect (Figure 5d). In comparison, a red shift of the LSPR band was observed for the Au–Cu alloy NPs, which is also evidence of alloying (Figure 5d and Figure S4 in the SI).²⁶ Characterizations of the photocatalysts, however, could not provide a direct explanation for the dramatic change in product selectivity. To gain insight into the reaction pathway of the process with the alloy photocatalyst, reductions of the possible intermediates (nitrosobenzene, phenylhydroxylamine, and their mixture) were conducted using $\text{Au}_{2.6}\text{Cu}_{0.4}@\text{ZrO}_2$ or monometallic $\text{Au}_{3.0}@\text{ZrO}_2$ as the catalyst, with the other experimental conditions maintained identical to those for the nitrobenzene reduction. The results are presented in Table 1. As shown in entries 1 and 2, when nitrosobenzene was the reactant, azoxybenzene was the main product no matter which catalyst was used, and the product selectivities were very similar. However, when phenylhydroxylamine was the reactant (entries 3 and 4), a striking difference in the product selectivities was observed: the main product with the alloy NP catalyst was azoxybenzene, while only a small fraction of azobenzene was detected (entry 3). The main product with the monometallic Au NP catalyst was azobenzene, and no

Table 1. Reaction Pathway Study of the Catalytic Performance Using $\text{Au}_{2.6}\text{Cu}_{0.4}@\text{ZrO}_2$ and Monometallic $\text{Au}_{3.0}@\text{ZrO}_2$ Catalysts with Various Intermediates as Substrates^a

entry	substrate	catalyst	conv. (%)	selectivities (%)		
				3	4	5
1 ^b	(1) Nitrosobenzene	Au–Cu	100	5	3	85
2 ^b	or (2) Phenylhydroxylamine	Au	100	4	4	83
3 ^c	(1)	Au–Cu	100	19	6	75
4 ^c	(2)	Au	100	15	85	0
5 ^c	1 + 2	Au–Cu	100	4	3	93
6 ^c	1 + 2	Au	100	8	92	0
7 ^d	4	Au–Cu	70	100	0	0
8 ^d	4	Au	55	10 ^e	–	0

^aThe reactions were conducted under an argon atmosphere at 40 °C using 2 mL of isopropyl alcohol mixed with 0.025 mmol of KOH, 0.1 mmol of substrate (for entries 5 and 6, 0.05 mmol of substrate 1 and 0.05 mmol of substrate 2 were used), and 50 mg of catalyst at an irradiation intensity of 0.5 W/cm² for the indicated reaction times. The conversions and selectivities were calculated from the amounts of products formed and reactants converted as measured by gas chromatography (GC). ^bReaction time = 3 h. ^cReaction time = 1 h. ^dReaction time = 16 h. ^eThe other product selectivity was 90% hydroazobenzene.

azoxybenzene was observed (entry 4). The reaction proceeded rapidly and was complete within 1 h, indicating that phenylhydroxylamine was highly reactive. The small amounts of aniline in the product (19% and 15%) could have formed via a disproportionation pathway simultaneously with the coupling route as proposed in Figure 1, which is based on the literature.¹⁰

Further experiments using a mixture of nitrosobenzene and phenylhydroxylamine as the reactant gave similar results (Table 1, entries 5 and 6). The reaction between nitrosobenzene and phenylhydroxylamine occurred spontaneously (without catalyst) and rapidly as soon as they were mixed, yielding mainly azoxybenzene. Thus, we can exclude the formation of intermediates such as nitrosobenzene and phenylhydroxylamine in the reduction using $\text{Au}_{2.6}\text{Cu}_{0.4}@\text{ZrO}_2$ catalyst, because if they were formed in the reaction, either of them would result in the coupling products. Comparison of the results of entry 2 with those of entries 4 and 6 indicates that phenylhydroxylamine is the key intermediate to afford the main product azobenzene in the reaction catalyzed by monometallic Au NPs. Moreover, the Au–Cu alloy NPs can also catalyze the reduction of azobenzene to the sole product aniline with 100% selectivity within 16 h under visible-light irradiation, whereas the pure Au NPs are slow to yield the aniline product even after prolonged reaction time (entries 7 and 8). This suggests that the

formation of aniline on the Au–Cu alloy surface is highly favored, while pure Au NPs exhibit a much weaker ability to catalyze the hydrogenation of azobenzene to aniline, causing the Au NP surface to exhibit selectivity for azobenzene in the reduction process.

We propose a reaction pathway that would explain this difference, as shown in Figure 6. Analysis confirmed that the

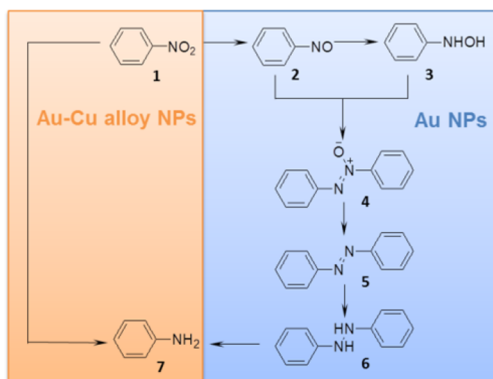


Figure 6. Proposed reaction pathway for the reduction of nitrobenzene in the present study.

monometallic Au NPs catalyzed the reaction via Haber's coupling route. By this pathway, the final product aniline was obtained mainly after the coupling step (azoxy \rightarrow azo \rightarrow hydrazo \rightarrow aniline). In the reaction system of the present study, H–Au species form on the surface of metal NPs as isopropanol provides hydrogen while being oxidized to acetone.¹² The H–Au species can react with nitrobenzene to yield nitrosobenzene. According to Haber's mechanism, nitrosobenzene is a reactive intermediate that is transformed to phenylhydroxylamine rapidly.^{10,11} This is the reason why nitrosobenzene was not detected during the reaction. The high concentration of phenylhydroxylamine favors the formation of azobenzene on the Au NPs (Table 1, entries 4 and 6). Blaser proposed that Haber's coupling route is favored under basic conditions.¹⁰ This is certainly true in the case of the monometallic Au catalyst. When the Au–Cu alloy NPs were used as the photocatalyst, nitrobenzene was transformed directly to aniline as the sole product, and we did not detect any byproduct such as azobenzene or other intermediates during the reaction. The detailed mechanistic understanding of this phenomenon is still unclear and may need further future work to explore in detail. Interestingly, even under basic conditions (when KOH was added to the reaction system) the reduction catalyzed by Au–Cu alloy NPs followed the direct reduction route.

To further understand the reason why aniline was the sole product of the reaction catalyzed by Au–Cu alloy NPs, we performed a density functional theory (DFT) simulation study of the adsorption of the reactant nitrobenzene and the product aniline on the surfaces of Au and Au–Cu clusters, respectively (Figure 7 and Table S1 in the SI). The DFT simulation results indicate that both the reactant nitrobenzene and the product aniline adsorb more strongly to the Au–Cu alloy surface than to the pure Au surface. The interaction of the N atom of the nitrobenzene or aniline molecule with a Cu atom in the Au–Cu alloy NPs is much stronger than that with Au atoms on the NP surface. This immobilizes the reactant molecules adsorbed at Cu atom sites on the alloy NP surface. Mobility of the reactant

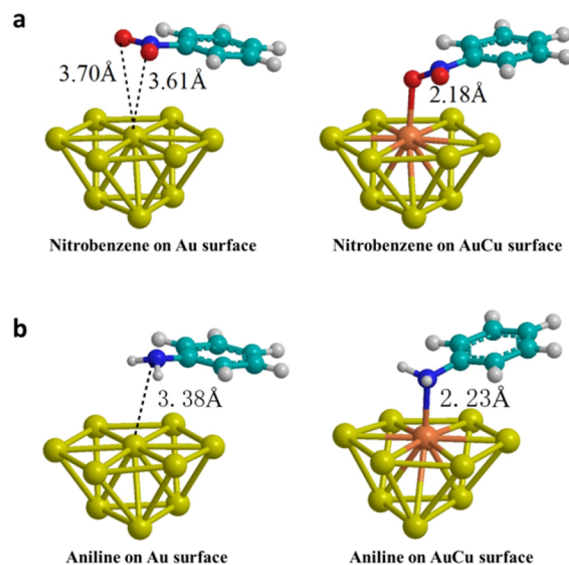


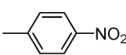
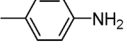
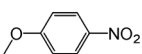
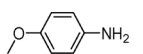
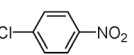
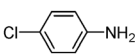
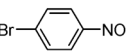
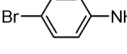
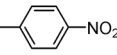
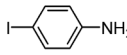
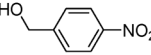
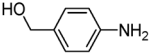
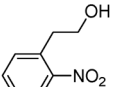
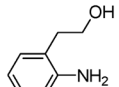
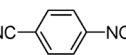
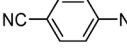
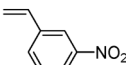
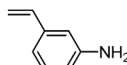
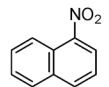
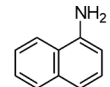
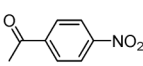
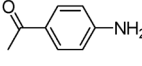
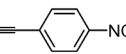
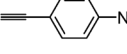
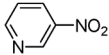
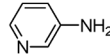
Figure 7. DFT-simulated (a) nitrobenzene and (b) aniline on the Au and Au–Cu alloy surfaces. The nitrobenzene molecule has much stronger interaction with the Au–Cu alloy surface than with the pure Au surface, as shown in panel (a). When an aniline molecule is adsorbed on the Au–Cu alloy surface, the N atom in the aniline molecule is attracted to the Cu atom, and the length of the N–Cu bond is 2.23 Å. However, when an aniline molecule is close to the surface of the Au NP, the N atom is repelled, as shown in panel (b). The interaction of the N atom of the nitrobenzene or aniline molecule with a Cu atom in the Au–Cu alloy NP is much stronger than that with Au atoms on the Au NP surface.

molecules is a prerequisite for the coupling reaction, so in contrast to the Au–Cu alloy, the reactant molecules (intermediate molecules with N atoms) on a pure Au surface are labile and can move for coupling. The reactant molecules immobilized on the Cu atoms are directly reduced to aniline. The product aniline is also much more stable on the Au–Cu alloy surface than on the pure Au surface. The simulation results confirm that the formation of aniline on the Au–Cu alloy surface is favored thermodynamically compared with that on the Au NP surface. Moreover, in regard to the difference between the surface electronic properties of the alloy NPs and pure Au NPs, the electronegativity of Au (2.54) is much higher than that of Cu (1.90).²⁷ There are electron-rich sites of Au and slightly positively charged sites of Cu on the surface of the alloy NPs. The interaction between aniline and the positively charged sites is stronger than that between aniline and the pure Au NP surface. Hence, thermodynamically the formation of aniline on the alloy surface is more favorable than that on the pure Au surface, and thus, alloying Au with Cu in the present study always enhances the product selectivity for aniline.

The isopropyl alcohol was the reducing agent and was first oxidized to acetone, yielding H–Au NP^{12,28} or H–Cu NP species.²⁰ Given the high Au content in the alloy NPs, the H–Au NP species are considered to play the major role in reacting with the oxygen atoms of N–O bonds in the nitrobenzene to induce the reduction on the surface of the alloy NPs.

The general applicability of the Au–Cu alloy NP-photocatalyzed reduction of nitroaromatics was studied. Table 2 shows the results for the reduction of nitroaromatics to anilines using the Au_{2.6}Cu_{0.4}@ZrO₂ catalyst under visible-light irradiation and in the dark. Visible-light irradiation promoted each reaction, as the yield of the light-irradiated reaction was much

Table 2. Photocatalytic Reduction of Substituted Nitroaromatics Using the $\text{Au}_{2.6}\text{Cu}_{0.4}@\text{ZrO}_2$ Catalyst^a

Entry	Reactant	Product	Yield (%)
1			Light 95
		Dark	36
2			Light 89
		Dark	40
3			Light 63
		Dark	24
4			Light 90
		Dark	20
5			Light 40
		Dark	0
6			Light 45
		Dark	8
7			Light 100
		Dark	23
8			Light 100
		Dark	34
9			Light 95
		Dark	29
10			Light 85
		Dark	36
11 ^b			Light 65
		Dark	0
12 ^c			Light 64
		Dark	0
13 ^d			Light 45
		Dark	0

^aThe reactions were conducted under an argon atmosphere at 40 °C using 2 mL of isopropyl alcohol mixed with 0.025 mmol of KOH, 0.1 mmol of reactant, and 50 mg of $\text{Au}_{2.6}\text{Cu}_{0.4}@\text{ZrO}_2$ catalyst. The irradiation intensity was 0.5 W/cm², and the reaction time was 6 h. In all cases, the product selectivity for the aniline was 100%. The yields were calculated from the amounts of products formed and reactants converted as measured by GC. ^b100 mg of $\text{Au}_{2.6}\text{Cu}_{0.4}@\text{ZrO}_2$ catalyst was used, and the reaction temperature was 60 °C. ^c0.05 mmol of reactant, 2 mL of 1:1 isopropyl alcohol/tetrahydrofuran mixed solvent, and 100 mg of $\text{Au}_{2.6}\text{Cu}_{0.4}@\text{ZrO}_2$ catalyst were used. The reaction temperature was 60 °C, and the reaction time was 48 h. ^dThe reaction temperature was 60 °C, and the reaction time was 16 h.

higher than that of the reaction in the dark in every case. The products were the corresponding anilines, and no coupling products such as azo or azoxy compounds were detected. For the reduction of halogen-containing nitroaromatics, dehalogenation could sometimes be inevitable. In our case, the dehalogenation was suppressed, and quantitative conversion of these substrates was realized (entries 3–5).

The most challenging substrates are those that bear other easily reducible moieties. The reduction of these substrates allows production of important products: functionalized anilines. The $\text{Au}_{2.6}\text{Cu}_{0.4}@\text{ZrO}_2$ catalyst was not only observed

to be able to reduce nitro groups in the presence of alkenes (Table 2, entry 9) but could also reduce them in the presence of alkynes without detectable concurrent reduction of the unsaturated unit (entry 12). Nitrile and keto substituents and heteroarene groups were unaffected as well. Paracetamol (*N*-acetyl-*p*-aminophenol) is a major ingredient in numerous analgesic, cold, and flu remedies.²⁹ Typically, it is produced by reduction of 4-nitrophenol to 4-aminophenol followed by acetylation with acetic anhydride.²⁹ The reduction of 4-nitrophenol is the key step, and H₂ or NaBH₄ are the widely used reductants. The reaction can be easily monitored by UV/vis spectroscopy.^{30–32} In the present study, we found that 4-nitrophenol can be selectively reduced to 4-aminophenol using the Au–Cu alloy NP catalyst under irradiation (Figure S5 in the SI).

Evidently, the Au–Cu alloy NP catalyst is an efficient photocatalyst for selective reduction of nitroaromatics directly to functionalized anilines using visible light under mild reaction conditions compared with those in the reported elegant works.^{3–6} To achieve a higher catalytic rate, we simply increased the reaction temperature slightly from 40 to 60 °C for several substrates under typical reaction conditions (Table S2 in the SI). The reactions achieved 100% conversion within 45 min and still maintained the high chemoselectivity to reduce the nitro groups. This is due to the continuum of metal electron energy levels in the metal NP photocatalysts, which provides the capacity to couple the stimuli of irradiation and heat to drive reactions.^{33,34} This is an apparent merit compared with traditional heterogeneous catalysts and semiconductor photocatalysts.

In the photocatalytic process, the light drives the reduction and reductive coupling by exciting metal electrons, and these light-excited electrons (so-called hot electrons) provide the activation energy required for cleavage of the N–O bond. This conclusion is supported by the fact that the catalytic activity of the $\text{Au}_{2.6}\text{Cu}_{0.4}@\text{ZrO}_2$ photocatalyst for the reduction of nitrobenzene to aniline significantly depends on the irradiation intensity (Figure 8a). When the irradiation intensity was raised, the aniline yields increased, and at higher intensity the contribution of irradiation to the overall reaction rate was greater. A higher irradiation intensity excites more hot electrons to populate levels above the Fermi level of the metal NPs, which can facilitate the reactions, as reported for Au NPs.^{33–39} Moreover, when the irradiation intensity was maintained constant, we found that the reaction rate was higher at the wavelength absorbed more strongly by the catalyst for a number of reductions, as shown in the action spectra of the reactions.^{20,35–37} Such an action spectrum is shown in Figure 8b. In the action spectrum, the apparent quantum yield (AQY) of the reduction is closely related to the irradiation wavelength. The action spectrum for the reduction of nitrobenzene to aniline using the $\text{Au}_{2.6}\text{Cu}_{0.4}@\text{ZrO}_2$ photocatalyst shows that the AQY for aniline matches well the light absorption of the alloy NP catalyst. The highest yield is achieved under irradiation at the wavelength where the alloy NPs have the most intense absorption due to the LSPR effect.

The hot electrons activate the reaction by two mechanisms: First, the hot electrons can be transferred to the molecular orbital of the reactant molecule adsorbed on the metal NP surface⁴⁰ that is associated with the chemical bonds to be cleaved (here the N–O bonds). There is an energetic requirement for hot electron transfer: the hot electrons must have an energy above a threshold that depends on the energy

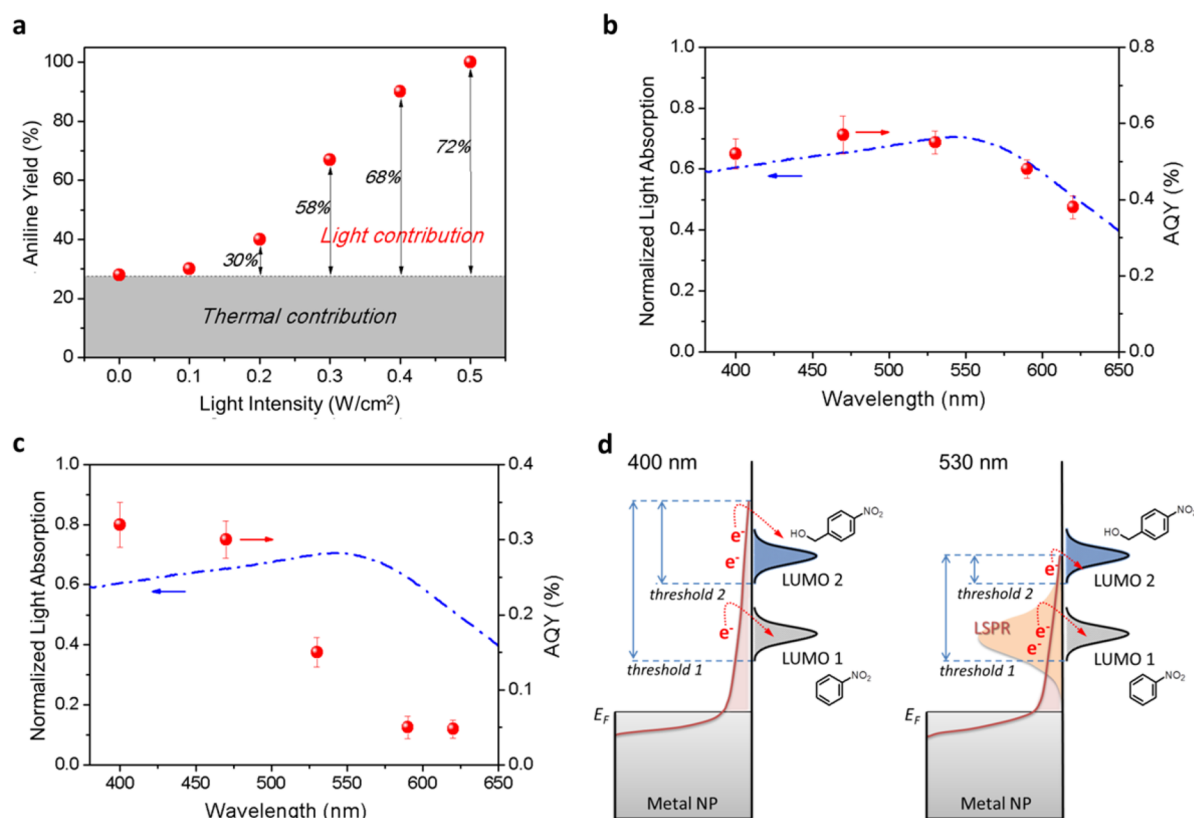


Figure 8. Impact of light intensity and wavelength. (a) Dependence of the catalytic activity of the $\text{Au}_{2.6}\text{Cu}_{0.4}@\text{ZrO}_2$ photocatalyst for the reduction of nitrobenzene to aniline on the intensity of the light irradiation. The percentages inside the figure show the contributions of the light irradiation effect. (b) Action spectrum for the photocatalytic reduction of nitrobenzene using the $\text{Au}_{2.6}\text{Cu}_{0.4}@\text{ZrO}_2$ catalyst. (c) Action spectrum for the photocatalytic reduction of 4-nitrobenzyl alcohol using the $\text{Au}_{2.6}\text{Cu}_{0.4}@\text{ZrO}_2$ catalyst. (d) Hot electron distributions of metal NPs under irradiation at different wavelengths (400 and 530 nm) and schemes showing how the hot electrons contribute to activation of nitrobenzene and 4-nitrobenzyl alcohol reactant molecules. The hot electrons with energies above the energy of the LUMO of the molecules adsorbed on the alloy NP can be transferred into those orbitals, thereby potentially inducing reaction. The calculated HOMOs and LUMOs for nitrobenzene and 4-nitrobenzyl alcohol are shown in Figure S6 in the SI. The LUMO of 4-nitrobenzyl alcohol (LUMO 2) is higher than that of nitrobenzene (LUMO 1), resulting in two thresholds (thresholds 1 and 2) for activation of the molecules. Thus, LUMO 2 requires light excitation of energetic electrons to higher energy levels to activate the molecule. As the strong chemisorption of adsorbates involves resonant electronic transitions between hybridized metal and adsorbate states, the relative positions of LUMO 1 for nitrobenzene and LUMO 2 for 4-nitrobenzyl alcohol with respect to the Fermi level are only qualitative and schematically show the relative positions of the LUMOs of the chemisorbed adsorbates.

level of the molecular orbital associated with the N–O bonds.⁴¹ Hot electrons with sufficient energy can be transferred to the reactant molecules and weaken the N–O bonds, resulting in the reaction. Second, although low-intensity illumination of plasmonic metal NPs most likely does not play a role in inducing chemistry, particularly in continuous flow,⁴² the hot electrons can dissipate their energy via electron–phonon interactions to heat the lattice of the NPs,⁴¹ especially when the hot electrons do not have sufficient energy for the direct transfer to the adsorbed reactant molecules.⁴¹

If the light energy absorbed by the hot electrons dissipates entirely as heat in the NPs, the AQY depends on the light absorption at all wavelengths. The higher AQY is observed at the wavelength more strongly absorbed by the catalyst. Nonetheless, if the energy threshold for the hot electron transfer is low, such a dependence can also be observed. The reduction of nitrobenzene is likely to have a low energy threshold (Figure 8b).

Figure 8c displays a different action spectrum for the reaction using 4-nitrobenzyl alcohol as the substrate: the reaction AQY value is greater at shorter wavelengths (e.g., 400 and 470 nm)

although the strongest light absorption of the catalyst appears at 560 nm. It is also noted that the AQY values at wavelengths of 590 and 620 nm are approximately one-sixth of the values at 400 and 470 nm, while the light absorption at the longer wavelengths is about 20% less than that at the shorter wavelengths. Hence, the photothermal effect cannot have induced such a large difference in the AQY values. Actually, the AQY values at wavelengths of 590 and 620 nm provide an approximate measure of the photothermal effect. Evidently for this reaction, cleavage of the N–O bonds is predominantly driven by hot electron transfer.

We noted that the yield of 4-nitrobenzyl alcohol reduction is much lower than that of nitrobenzene reduction (Table 2). This means that it is more difficult to cleave the N–O bonds in 4-nitrobenzyl alcohol with hot electrons excited by the LSPR light absorption compared with the corresponding process in nitrobenzene. The alcohol group substituted on the aromatic ring raises the energy of the lowest unoccupied molecular orbital (LUMO) associated with the N–O bonds (Figure 8d). The hot electrons generated in the metal by shorter-wavelength irradiation have enough energy to effectively activate 4-nitrobenzyl alcohol molecules for reaction (Figure 8d, left). It

is therefore rational that the N–O bond-cleaving reaction is predominately driven by hot electron transfer with a high energy threshold in this case.

When the hot electrons are transferred into the LUMO of the reactant molecules adsorbed on the metal NPs,^{35,37,39,42–44} which is associated with the N–O bonds, the bonds are weakened and the reduction is activated. Only the hot electrons with energy above a threshold that depends on the energy of the LUMO can be injected into the adsorbed reactant LUMO to induce the reaction (see Figure 8d).⁴⁰ The calculated energy of the LUMO of 4-nitrobenzyl alcohol (–2.7 eV) is higher than that of nitrobenzene (–2.9 eV), and thus, the Fermi level of Au, which is –5.1 eV, lies about 2.4 and 2.2 eV below the LUMO levels of 4-nitrobenzyl alcohol and nitrobenzene, respectively (Figure S6 in the SI). Only the hot electrons with energies of at least 2.4 eV above the Au Fermi level can induce the reaction of 4-nitrobenzyl alcohol. The Fermi level of the alloy NPs is slightly higher than that of Au, and thus, the energy required for the injection is reduced (<2.4 eV). Shorter wavelengths more effectively generate hot electrons with sufficient energy to be transferred (Figure 8d, left). The light absorption due to the LSPR effect is intense and can excite a large number of metal electrons, but only to energy levels about 2 eV above the Fermi level (Figure 8d, right). Hence, the LSPR absorption is not as effective as the absorption of shorter wavelengths in driving the reduction of 4-nitrobenzyl alcohol, while it effectively drives the reduction of nitrobenzene because nitrobenzene possesses a lower LUMO energy. We have to bear in mind that the above discussion of the energetics of the reaction systems are semiquantitative since the influence of the reactant adsorption is not included. Another possible mechanism such as direct charge transfer (direct excitation of an electron to the LUMO without the formation of an excited electron distribution in the metal) may also be involved in the reaction.⁴⁵ The present study has limited capacity to distinguish between indirect and direct charge transfer mechanisms for the reactions. Nonetheless, the discussion reveals that the reduction reaction is mainly driven by hot electron transfer from the alloy NP to the LUMO associated with the N–O bonds.

It is noted that high AQY values were found in the short-wavelength range of the action spectra. In this range (400–450 nm), one photon can excite an electron (interband transition) to a higher energy level than those excited by LSPR absorption in Au–Cu NPs at the expense of LSPR excitation. These high-energy hot electrons can subsequently generate more hot electrons with lower energy by electron–electron collisions. The higher AQY values suggest that the short-wavelength photons can result in more effective adsorbate-specific energy transfer to activate the N–O bonds on the NP surface. It has been reported that size of the metal NP affects wavelength-dependent photocatalytic reactions.⁴⁶ Small NPs (approximately 5.0 nm) have large fractions of surface atoms, making photon absorption likely to occur at surface atoms that are directly bonded to adsorbates, which may facilitate the direct photoexcitation of metal–adsorbate bonds to enhance the photocatalytic reaction on the NP surface under irradiation.⁴⁶

To further investigate the hot electron transfer process on the Au–Cu alloy NP surface, we simulated the molecular orbitals involved in the hot electron transfer processes for nitrobenzene and 4-nitrobenzyl alcohol reactant molecules adsorbed on the Au–Cu cluster surface (see Figure S7 in the SI). The details of the time-dependent DFT (TD-DFT) results are listed in Tables S3–S6 in the SI. The change in charge

density distribution indicates electron transfer from the metal NP to the LUMO of the adsorbed reactant molecules under irradiation. These simulation results provide insight into the dependence of the catalytic activity on the intensity and wavelength of the incident light.

CONCLUSIONS

This study has demonstrated that Au–Cu alloy NPs supported on ZrO₂ are an excellent photocatalyst for the selective reduction of nitroaromatics to the corresponding functionalized anilines as the sole products driven by visible-light irradiation without requiring intensive heating and pressurized reagents. The reasons for the high efficiency of the photocatalytic reduction under these comparatively benign conditions have been analyzed. During the photocatalytic reductions using this catalyst, the nitro group is transformed to an amino group directly rather than in a stepwise manner via a series of intermediates as described by Haber. The interaction between the nitro group and copper atoms is stronger than that between the nitro group and gold atoms, immobilizing the reactant. This effect facilitates direct reduction of the nitro group to an amino group and impedes the coupling reaction between two intermediate molecules. The change in reaction pathway and mild reaction conditions are the essential reasons for the high chemoselectivity for the anilines. The catalytic reaction rate can be further optimized by a slight increase in the reaction temperature, while the high chemoselectivity for reduction of the nitro groups is maintained. This study reveals that product chemoselectivity may be engineered simply by tailoring the bimetallic alloy NPs of the photocatalysts. This approach represents a promising new direction in the area of photocatalytic chemical transformations.⁴⁵ The knowledge acquired in this study could be useful in the development of new heterogeneous photocatalysts for the production of important chemicals, functionalized anilines and others, and in understanding photocatalytic systems for organic reactions.

EXPERIMENTAL SECTION

Chemicals. Zirconium(IV) oxide (ZrO₂, <100 nm particle size, TEM), gold(III) chloride hydrate (HAuCl₄·xH₂O, 99.999% trace metals basis), sodium borohydride (NaBH₄, ≥98.0%), copper(II) nitrate hydrate (Cu(NO₃)₂·xH₂O, ≥99.9% trace metals basis) were used. All of the chemicals employed in the experiments were purchased from Sigma-Aldrich (unless otherwise noted) and used as received without further purification. The water used in all of the experiments was prepared by passage through an ultrapurification system.

Preparation of Catalysts. As a typical example, the Au_{2.6}Cu_{0.4}@ZrO₂ catalyst was prepared as follows: ZrO₂ powder (1.0 g) was dispersed in a mixture of HAuCl₄ (13.2 mL, 0.01 M) and Cu(NO₃)₂ (6.25 mL, 0.01 M) aqueous solutions under magnetic stirring at room temperature. An aqueous solution of lysine (3 mL, 0.1 M) was then added to the mixture with vigorous stirring for 30 min, and the pH was 8–9. To this suspension was added a freshly prepared aqueous solution of NaBH₄ (2 mL, 0.35 M) dropwise. The mixture was aged for 24 h, and then the solid was separated by centrifugation, washed with water (three times) and ethanol (once), and dried at 60 °C in a vacuum oven for 24 h. The dried powder was subjected to thermal treatment in a mixture of H₂ (5 vol %) and Ar at 450 °C for 0.5 h. The obtained powder was used directly as the Au_{2.6}Cu_{0.4}@ZrO₂ catalyst. All

of the other catalysts were prepared via the same methods with different quantities of HAuCl_4 and $\text{Cu}(\text{NO}_3)_2$ aqueous solutions.

Characterization of Catalysts. The sizes, morphologies, and compositions of the catalyst samples were characterized by TEM using a JEOL 2100 transmission electron microscope equipped with a Gatan Orius SC1000 CCD camera and an Oxford X-Max EDS instrument. The Au and Cu contents of the prepared catalysts were determined by EDS technology using an EDS attachment to an FEI Quanta 200 environmental scanning electron microscope. Diffuse-reflectance UV/vis (DR-UV/vis) spectra of the sample powders were examined using a Varian Cary 5000 spectrometer with BaSO_4 as a reference. The light absorption data were normalized with OriginPro 8 software using the normalization method “normalize to [0, 1]”. The normalized data were plotted against wavelength to get the light absorption spectrum of the catalyst. XPS data were acquired using a Kratos Axis ULTRA X-ray photoelectron spectrometer incorporating a 165 mm hemispherical electron energy analyzer. The incident radiation was monochromatic Al $K\alpha$ X-rays (1486.6 eV) at 225 W (15 kV, 15 mA). Narrow high-resolution scans were run with 0.05 eV steps and a 250 ms dwell time. The base pressure in the analysis chamber was 1.0×10^{-9} Torr, and during sample analysis the pressure was 1.0×10^{-8} Torr. Peak fitting of the high-resolution data was carried out using the CasaXPS software.

Photocatalytic Reactions. A 20 mL Pyrex glass tube was used as the reaction container, and after the reactants and catalyst had been added, the tube was sealed with a rubber septum cap. The reaction mixture was stirred magnetically and irradiated using a Nelson halogen lamp with a wavelength in the range 400–800 nm (see Figure S8 in the SI) as the visible-light source, and the light intensity was measured to be 0.5 W/cm^2 . The temperature of the reaction system was carefully controlled with an air conditioner attached to the reaction chamber. The control reaction system in the dark was maintained at the same temperature to ensure that the comparison was meaningful. All of the reactions in the dark were conducted using a water bath placed above a magnetic stirrer to control the reaction temperature; the reaction tube was wrapped with aluminum foil to avoid exposure of the reaction mixture to light. At given irradiation time intervals, 0.5 mL aliquots were collected and then filtered through a Millipore filter (pore size $0.45 \mu\text{m}$) to remove the catalyst particulates. The liquid-phase products were analyzed by gas chromatography (GC) using an Agilent 7820A gas chromatograph with an HP-5 column to measure the changes in the concentrations of reactants and products. An Agilent HP5977A mass spectrometer attached to an Agilent 7890B gas chromatograph with an HP-5MS column was used to identify the products. The acetone concentration was tested using an Agilent 6890 gas chromatograph with a DB-Wax column.

Typical reaction conditions were as follows: 2 mL of a 0.05 M solution of nitrobenzene in isopropyl alcohol (IPA) (0.1 mmol), 0.25 mL of a 0.1 M solution of KOH in IPA (0.025 mmol), and 50 mg of catalyst were added to the reaction tube, and the reaction was run at a temperature of 40°C under a 1 atm argon atmosphere for a reaction time of 6 h. The reactions with other substrates were conducted under similar methods with some conditions changed slightly as noted in Table 2.

Light-emitting diode (LED) lamps (Tongyifang, Shenzhen, China) with wavelengths of 400 ± 5 , 470 ± 5 , 530 ± 5 , 590 ± 5 , and 620 ± 5 nm were used as the light sources to investigate

the catalytic performance at different irradiation wavelengths (action spectrum experiments). The light intensity of the LED light sources used for the wavelength-dependent experiments was 0.2 W/cm^2 , and the light intensity was maintained constant for each wavelength-dependent experiment. The other reaction conditions were kept identical with the halogen lamp photocatalytic reactions. The apparent quantum yield was calculated as $\text{AQY} = [(Y_{\text{light}} - Y_{\text{dark}})/(\text{number of incident photons})] \times 100\%$, where Y_{light} and Y_{dark} are the number of products formed under light irradiation and in the dark, respectively. The number of products formed, Y , was calculated using the equation $Y = y \times (\text{moles of reactant}) \times \text{Avogadro constant}$, where y is the product aniline yield for the reaction.

■ ASSOCIATED CONTENT

Supporting Information

The Supporting Information is available free of charge on the ACS Publications website at DOI: 10.1021/acscatal.5b02643.

Figures S1–S8 and Tables S1–S7 (PDF)

■ AUTHOR INFORMATION

Corresponding Author

*E-mail: hy.zhu@qut.edu.au.

Notes

The authors declare no competing financial interest.

■ ACKNOWLEDGMENTS

The authors gratefully acknowledge financial support from the Australian Research Council (ARC DP110104990 and DP150102110).

■ REFERENCES

- (1) Blaser, H. U.; Siegrist, U.; Steiner, H.; Studer, M. In *Fine Chemicals through Heterogeneous Catalysis*; Sheldon, R. A., van Bekkum, H., Eds.; Wiley-VCH: Weinheim, Germany, 2001; pp 389–406.
- (2) Rosenblatt, D. H.; Burrows, E. P. *The Chemistry of Amino Nitroso and Nitro Compounds and their Derivatives*; Wiley: Chichester, U.K., 1982; p 1085.
- (3) Corma, A.; Serna, P. *Science* **2006**, *313*, 332–334.
- (4) Grirrane, A.; Corma, A.; Garcia, H. *Science* **2008**, *322*, 1661–1664.
- (5) Jagadeesh, R. V.; Surkus, A. E.; Junge, H.; Pohl, M. M.; Radnik, J.; Rabeah, J.; Huan, H. M.; Schunemann, V.; Bruckner, A.; Beller, M. *Science* **2013**, *342*, 1073–1076.
- (6) Westerhaus, F. A.; Jagadeesh, R. V.; Wienhöfer, G.; Pohl, M.-M.; Radnik, J.; Surkus, A.-E.; Rabeah, J.; Junge, K.; Junge, H.; Nielsen, M.; Brückner, A.; Beller, M. *Nat. Chem.* **2013**, *5*, 537–543.
- (7) Haber, F. Z. *Elektrochem. Angew. Phys. Chem.* **1898**, *4*, 506–514.
- (8) Makosch, M.; Sa, J.; Kartusch, C.; Richner, G.; van Bokhoven, J. A.; Hungerbühler, K. *ChemCatChem* **2012**, *4*, 59–63.
- (9) Liu, X.; Li, H. Q.; Ye, S.; Liu, Y. M.; He, H. Y.; Cao, Y. *Angew. Chem., Int. Ed.* **2014**, *53*, 7624–7628.
- (10) Blaser, H. U. *Science* **2006**, *313*, 312–313.
- (11) Corma, A.; Concepción, P.; Serna, P. *Angew. Chem., Int. Ed.* **2007**, *46*, 7266–7269.
- (12) Zhu, H. Y.; Ke, X. B.; Yang, X. Z.; Sarina, S.; Liu, H. W. *Angew. Chem., Int. Ed.* **2010**, *49*, 9657–9661.
- (13) Chen, X.; Zhu, H. Y.; Zhao, J. C.; Zheng, Z. F.; Gao, X. P. *Angew. Chem., Int. Ed.* **2008**, *47*, 5353–5356.
- (14) Sarina, S.; Waclawik, E. R.; Zhu, H. Y. *Green Chem.* **2013**, *15*, 1814–1833.
- (15) Wang, C.; Astruc, D. *Chem. Soc. Rev.* **2014**, *43*, 7188–7216.
- (16) Khanal, S.; Bhattarai, N.; McMaster, D.; Bahena, D.; Velazquez-Salazar, J. J.; Jose-Yacamán, M. *Phys. Chem. Chem. Phys.* **2014**, *16*, 16278–16283.

- (17) Liu, X.; Wang, A.; Li, L.; Zhang, T.; Mou, C. Y.; Lee, J. F. *J. Catal.* **2011**, 278, 288–296.
- (18) Xu, Z.; Lai, E.; Shao-Horn, Y.; Hamad-Schifferli, K. *Chem. Commun.* **2012**, 48, 5626–5628.
- (19) Wang, L.; Yang, J. C. *J. Mater. Res.* **2005**, 20, 1902–1909.
- (20) Guo, X. N.; Hao, C. H.; Jin, G. Q.; Zhu, H. Y.; Guo, X. Y. *Angew. Chem., Int. Ed.* **2014**, 53, 1973–1977.
- (21) Gonçalves, R. V.; Wojcieszak, R.; Wender, H.; Dias, C. S. B.; Vono, L. L. R.; Eberhardt, D.; Teixeira, S. R.; Rossi, L. M. *ACS Appl. Mater. Interfaces* **2015**, 7, 7987–7994.
- (22) Schünemann, S.; Dodekatos, G.; Tüysüz, H. *Chem. Mater.* **2015**, 27, 7743–7750.
- (23) Sugano, Y.; Shiraishi, Y.; Tsukamoto, D.; Ichikawa, S.; Tanaka, S.; Hirai, T. *Angew. Chem., Int. Ed.* **2013**, 52, 5295–5299.
- (24) Marimuthu, A.; Zhang, J.; Linic, S. *Science* **2013**, 339, 1590–1593.
- (25) Cano, I.; Huertos, M. A.; Chapman, A. M.; Buntkowsky, G.; Gutmann, T.; Groszewicz, P. B.; van Leeuwen, P. W. N. M. *J. Am. Chem. Soc.* **2015**, 137, 7718–7727.
- (26) Pramanik, S.; Mishra, M. K.; De, G. *CrystEngComm* **2014**, 16, 56–63.
- (27) Section 9, Molecular Structure and Spectroscopy; Electronegativity. In *CRC Handbook of Chemistry and Physics*, 84th ed.; Lide, D. R., Ed.; CRC Press: Boca Raton, FL, 2003; pp 9–74.
- (28) Abad, A.; Concepción, P.; Corma, A.; García, H. *Angew. Chem., Int. Ed.* **2005**, 44, 4066–4069.
- (29) Ellis, F. *Paracetamol: A Curriculum Resource*; Royal Society of Chemistry: Cambridge, U.K., 2002; pp 3–12.
- (30) Saha, A.; Adamcik, J.; Bolisetty, S.; Handschin, S.; Mezzenga, R. *Angew. Chem., Int. Ed.* **2015**, 54, 5408–5412.
- (31) Li, A.; Luo, Q.; Park, S.-J.; Cooks, R. G. *Angew. Chem., Int. Ed.* **2014**, 53, 3147–3150.
- (32) Wang, X.; Liu, D.; Song, S.; Zhang, H. *J. Am. Chem. Soc.* **2013**, 135, 15864–15872.
- (33) Linic, S.; Christopher, P.; Ingram, D. B. *Nat. Mater.* **2011**, 10, 911–921.
- (34) Christopher, P.; Xin, H. L.; Marimuthu, A.; Linic, S. *Nat. Mater.* **2012**, 11, 1044–1050.
- (35) Xiao, Q.; Jaatinen, E.; Zhu, H. Y. *Chem. - Asian J.* **2014**, 9, 3046–3064.
- (36) Xiao, Q.; Liu, Z.; Bo, A.; Zavahir, S.; Sarina, S.; Bottle, S.; Riches, J. D.; Zhu, H. Y. *J. Am. Chem. Soc.* **2015**, 137, 1956–1966.
- (37) Sarina, S.; Zhu, H. Y.; Xiao, Q.; Jaatinen, E.; Jia, J.; Huang, Y.; Zheng, Z.; Wu, H. *Angew. Chem., Int. Ed.* **2014**, 53, 2935–2940.
- (38) Sarina, S.; Zhu, H.; Jaatinen, E.; Xiao, Q.; Liu, H.; Jia, J.; Chen, C.; Zhao, J. *J. Am. Chem. Soc.* **2013**, 135, 5793–5801.
- (39) Long, R.; Li, Y.; Song, L.; Xiong, Y. *Small* **2015**, 11, 3873–3889.
- (40) Brus, L. *Acc. Chem. Res.* **2008**, 41, 1742–1749.
- (41) Smith, J. G.; Fauchaux, J. A.; Jain, P. K. *Nano Today* **2015**, 10, 67–80.
- (42) Kale, M. J.; Avanesian, T.; Christopher, P. *ACS Catal.* **2014**, 4, 116–128.
- (43) Zhao, L. B.; Huang, Y. F.; Liu, X. M.; Anema, J. R.; Wu, D. Y.; Ren, B.; Tian, Z. Q. *Phys. Chem. Chem. Phys.* **2012**, 14, 12919–12929.
- (44) Zhao, L. B.; Zhang, M.; Huang, Y. F.; Williams, C. T.; Wu, D. Y.; Ren, B.; Tian, Z. Q. *J. Phys. Chem. Lett.* **2014**, 5, 1259–1266.
- (45) Linic, S.; Aslam, U.; Boerigter, C.; Morabito, M. *Nat. Mater.* **2015**, 14, 567–576.
- (46) Kale, M. J.; Avanesian, T.; Xin, H.; Yan, J.; Christopher, P. *Nano Lett.* **2014**, 14, 5405–5412.